Supporting Information

Hardware Implementation of Photoelectrically-Modulated Dendritic Arithmetic and Spike-Timing-Dependent Plasticity Enabled by Ion-Coupling Gate-Tunable Vertical 0D-Perovskite/2D-MoS_2 Hybrid-Dimensional van der Waals Heterostructure

Yongchao Cheng, Kexiang Shan, Yan Xu, Junliang Yang, Jun He*, and Jie Jiang*

Hunan Key Laboratory of Super Microstructure and Ultrafast Process, School of Physics and Electronics, Central South University, Changsha 410083, China

E-mail addresses: jiangjie@csu.edu.cn; junhe@csu.edu.cn

Supplementary Note 1

In our device, polymer ion-gel electrolyte exhibits an ultra-high capacitance (21.7 μF/cm^2) at the lowest frequency of 4 Hz, as shown in Figure S1. Such a high capacitance is due to the mobile-ions-induced electric-double-layer (EDL) effect, which tends to more likely dominate the memristive effect under the low-voltage operation.[1] Generally, when the transistor is under the small voltage bias, the device operation tends to be electrostatic doping and it can be operated repeatedly.[2] As a contrast, if the transistor is under a large voltage bias, the device operation tends to be electrochemical doping and it is irreversible.[2] In order to further clarify the operation mechanism of our transistor under the low-voltage operation, a new device was measured to examine the repeatability of transfer characteristics. Figure S2 shows the transfer characteristics of the device for five successive measurements. It is clear that the transfer characteristics are almost unchanged, indicating that the device operation is reversible. Therefore, it can be concluded that the operation mechanism is electrostatic modulating rather than electrochemical doping in our transistor under this voltage condition.

Supplementary Figures

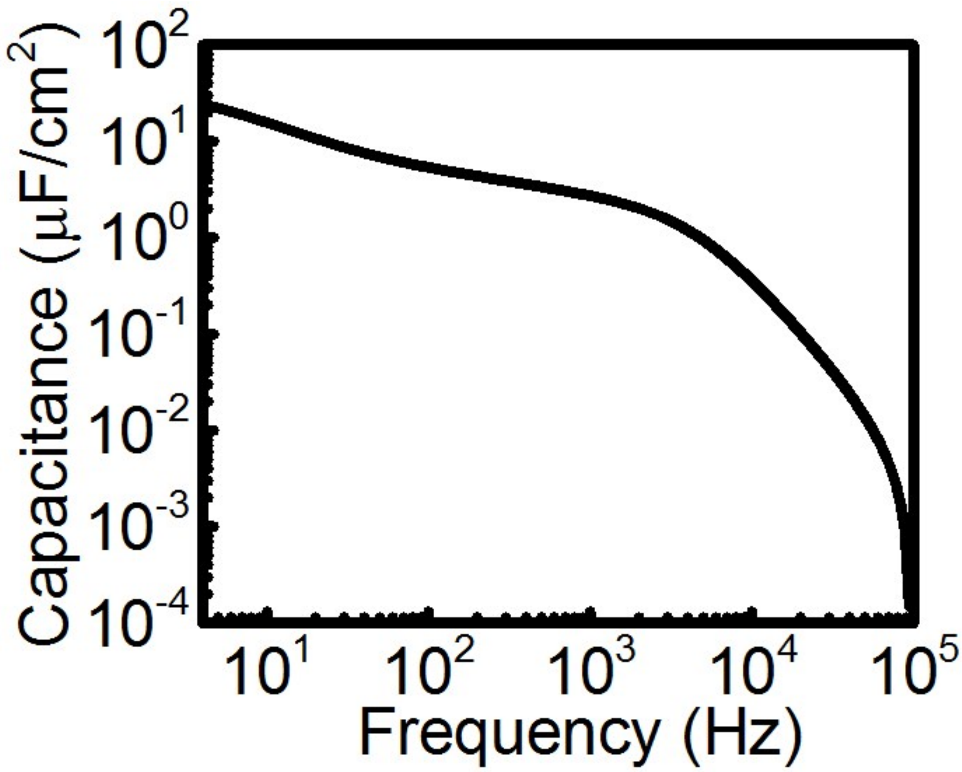

Figure S1. Specific capacitance of the ionic electrolyte film in our device as a function of frequency ranging from 4 Hz to 100k Hz.

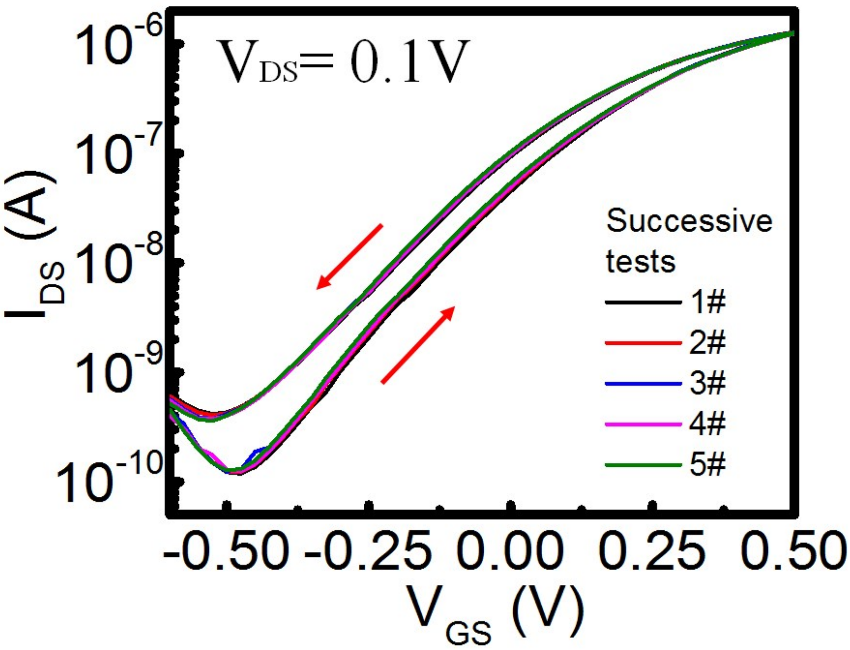

Figure S2. The transfer curves for five successive measurements.

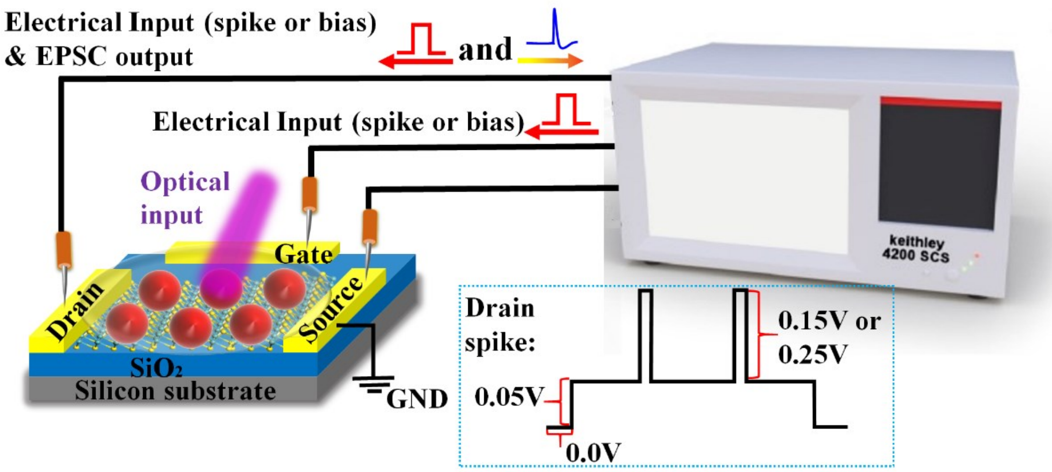

Figure S3. The device connections of EPSC measurements, and the pulse mode is applied to drain terminal in our device.

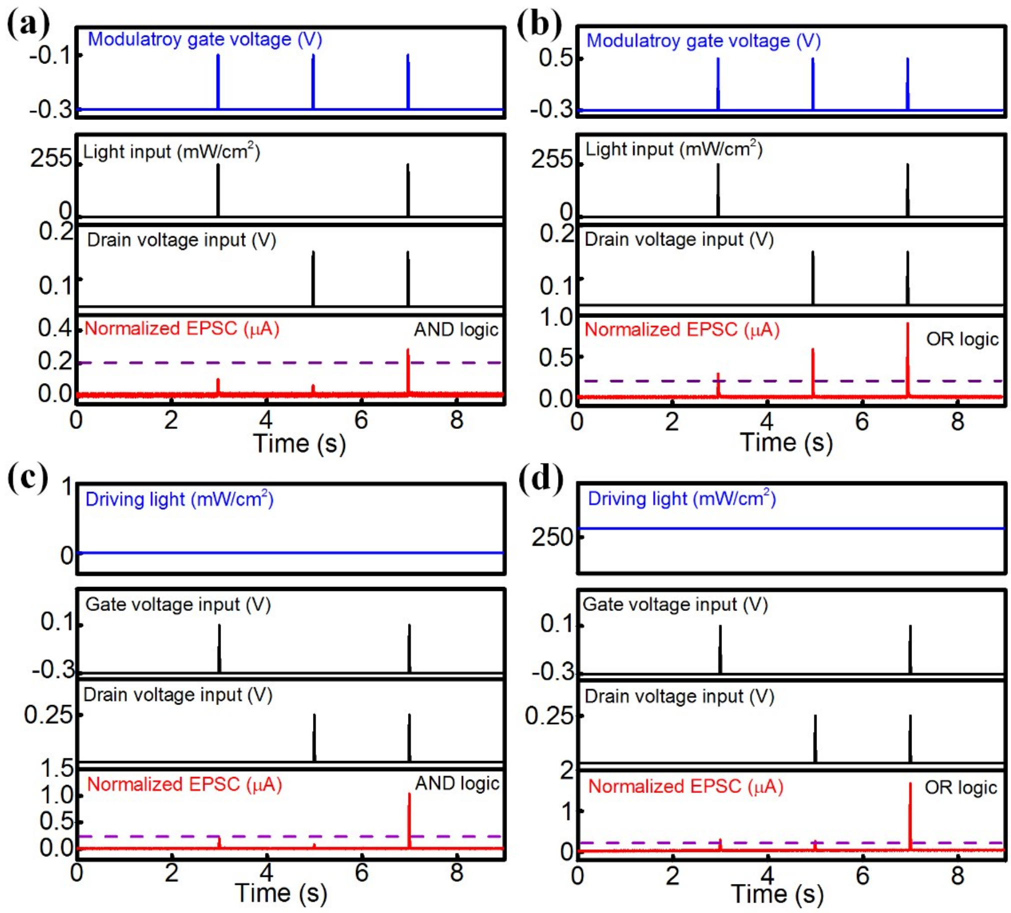

Supplementary Fig. S4. Spatial spiking logic responses of EPSCs by two presynaptic driving inputs and a modulatory gate voltage of (0.2 V, 10 ms) (a) and (0.8 V, 10 ms) (b), respectively. Spatial spiking logic responses of EPSCs by two presynaptic driving inputs and a driving light input: (c) 0mW/cm^2, (d) 255mW/cm^2, respectively.

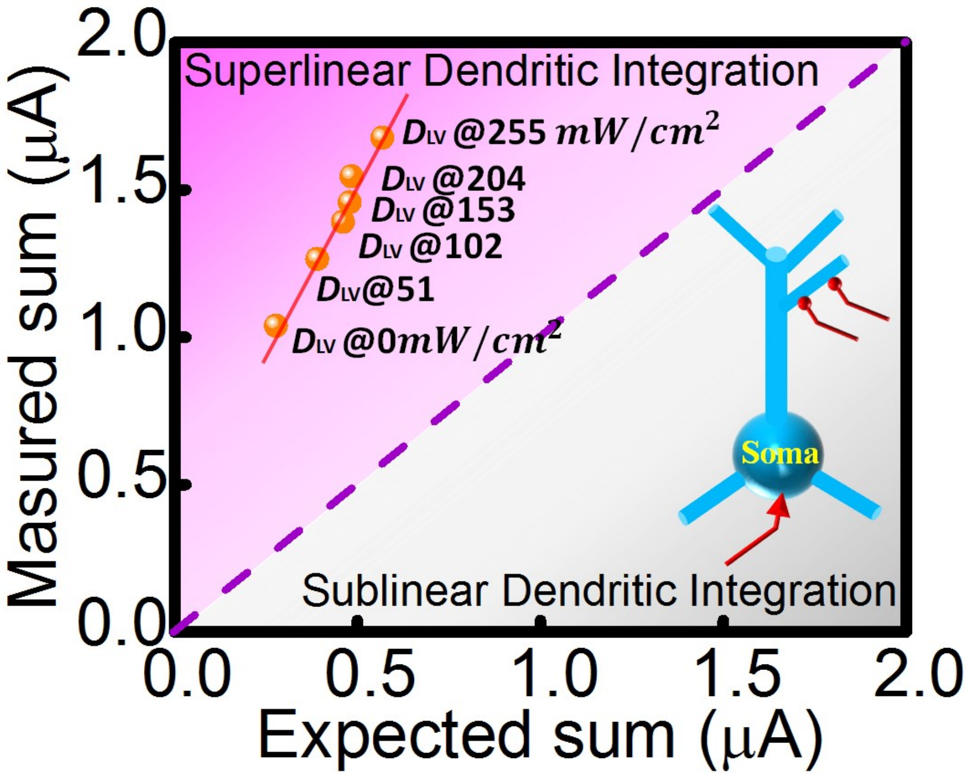

Supplementary Fig. S5. The superlinear dendritic integration is implemented by applying the intensity-varied light on the heterojunction channel to act as a driving input.

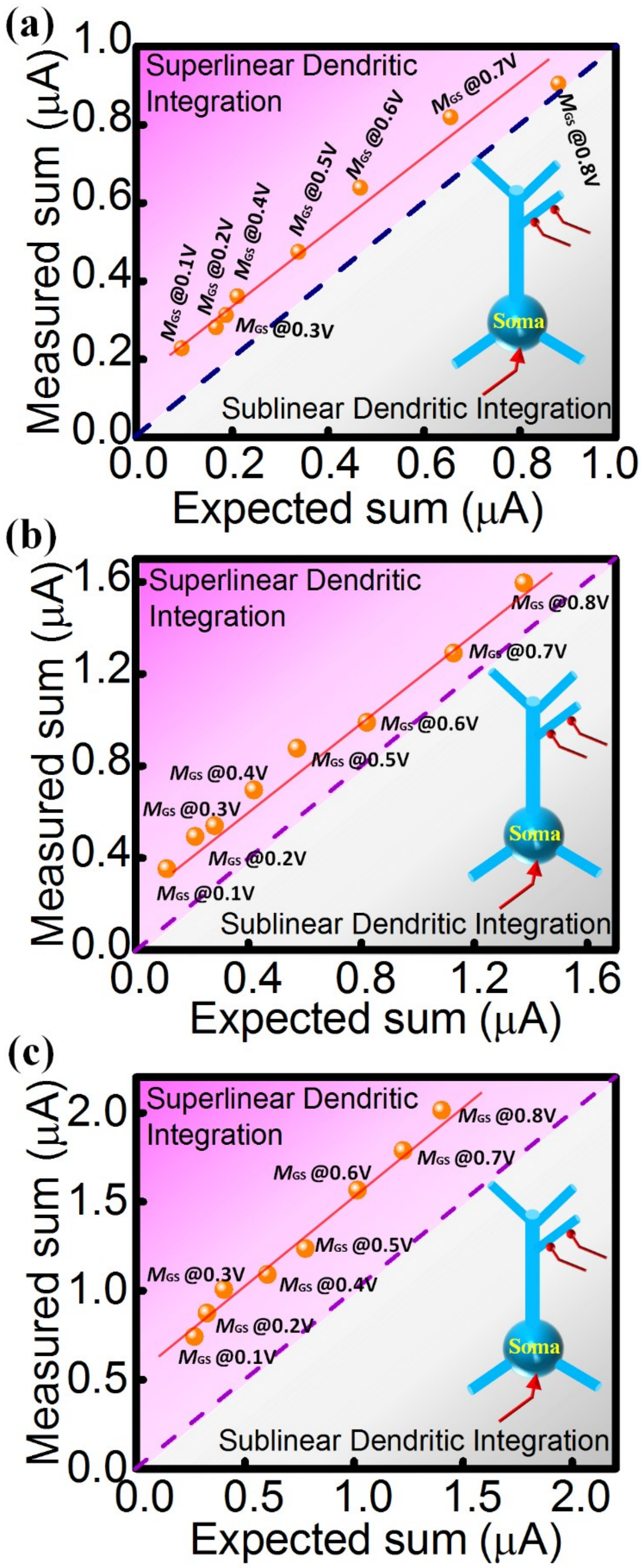

Supplementary Fig. S6. Under different drain input spikes (V_{ds}), the superlinear dendritic integration can also be realized by applying the different electrical spike on the coplanar gate to act as the modulatory input (M_{GS}): (a) for the V_{ds} = 0.1V, (b) for the V_{ds} = 0.2V, (c) for the V_{ds} = 0.3V, respectively.

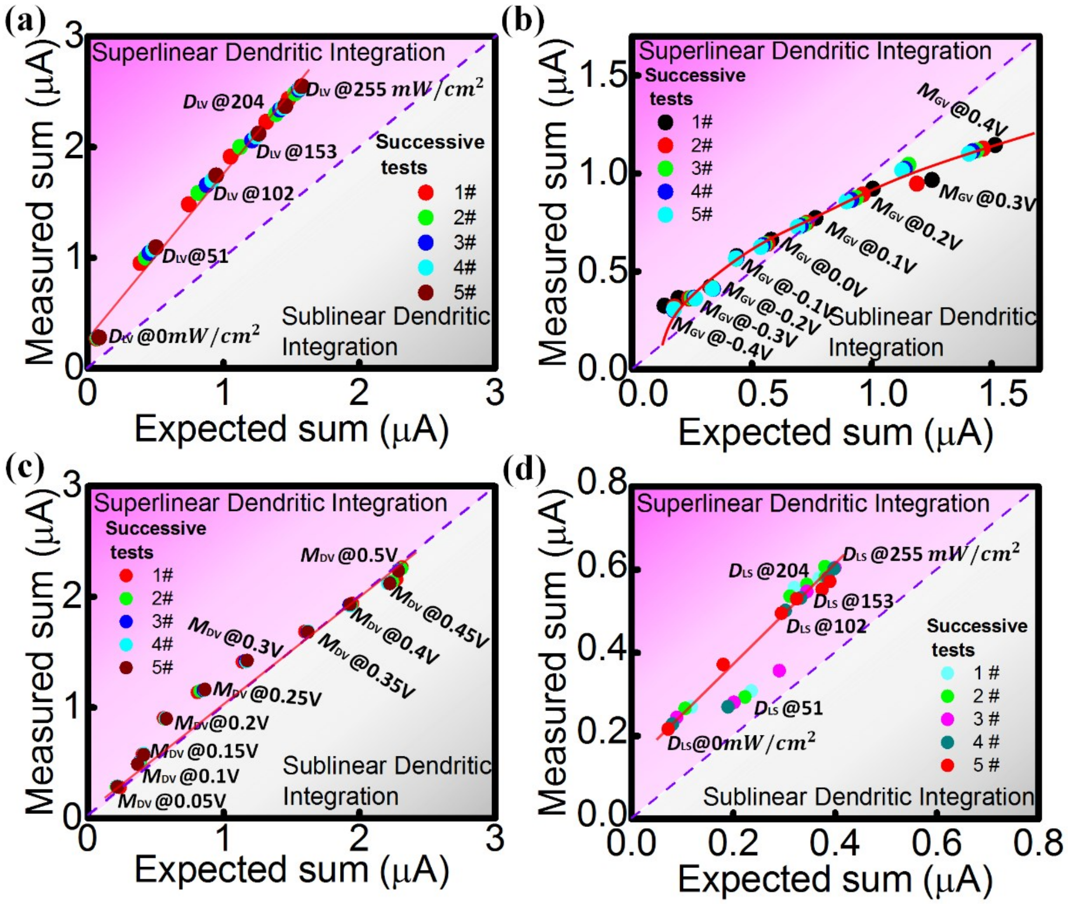

Figure S7. (a)-(d) Repeatability of different dendritic integration with five successive measurements on the same device. (a) The repeatability of superlinear dendritic integration modulated by changing the intensity of driving light input (D_{LV}). (b) The repeatability of sigmoidal nonlinear integration modulated by changing the modulatory gate voltage (M_{GV}). (c) The repeatability of linear dendritic integration modulated by changing the modulatory drain voltage (M_{DV}). (d) The repeatability of superlinear dendritic integration modulated by changing the intensity driving-light spike input (D_{LS}).

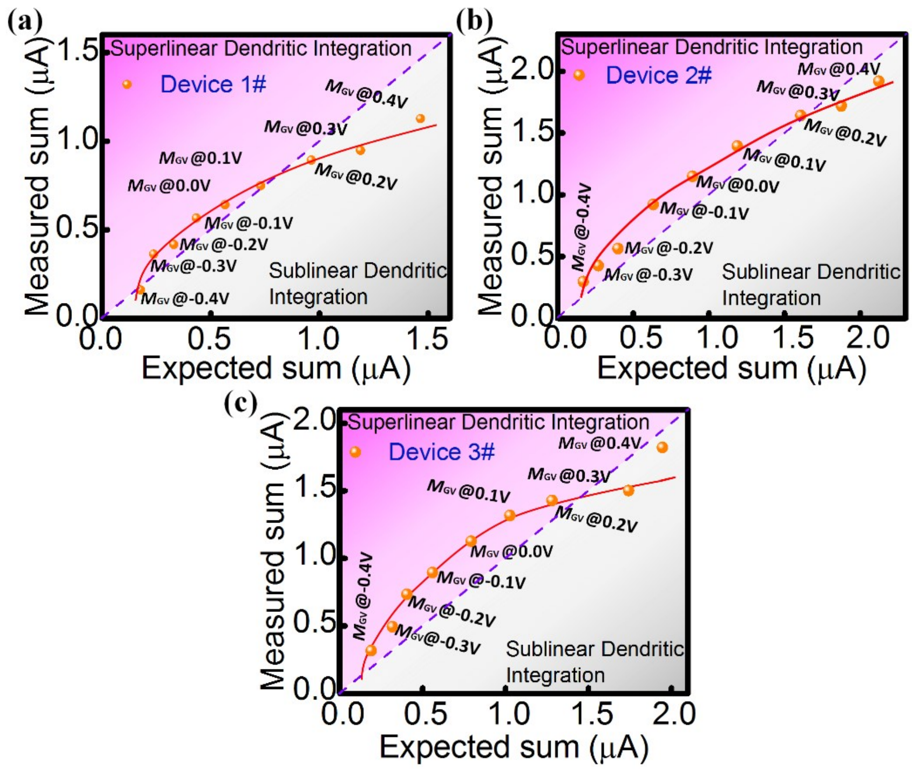

Figure S8. (a)-(c) Repeatability of sigmoidal nonlinear integration on device-to-device.

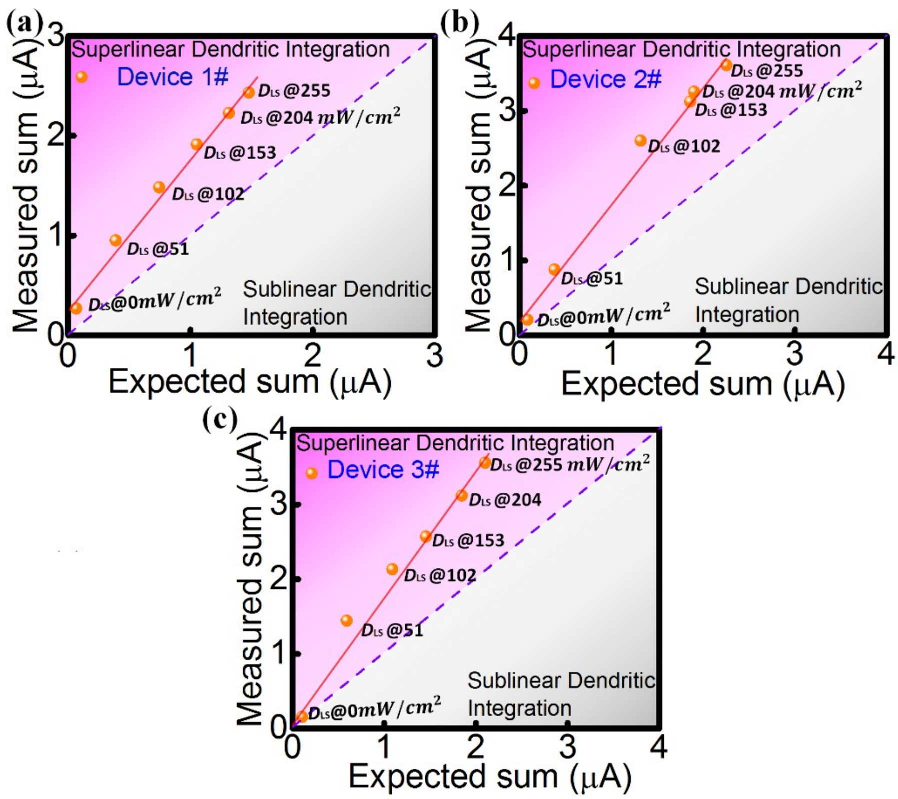

Figure S9. (a)-(c) Repeatability of superlinear dendritic integration on device-to-device.

Supplementary Note 2

At present, the underlying mechanism about these dendritic arithmetics is still under debate and the discussion about the relation between device physics and dendritic arithmetics may thus be unmature. Herein, we give our possible qualitative explanation for this issue:

(i) Firstly, as shown in Fig. S10 below, the Fig. S10a shows a schematic diagram for the two driving inputs of electrical gate and drain terminals. The channel would be pitched off if it gets saturated gradually. The top panel of Fig. S10b further shows the underlying energy diagram for the device without any biases. In this case, the electrons ejecting from source electrode need to overcome high Schottky barriers at the metal-channel(MoS_2) interface.[3, 4] If both the electrical gate and drain pulses are applied, the Fermi level will shift toward the conduction band and the source-to-drain energy-band difference will increase to be q[$V_{D(bias)}$+$V_{D(pulse)}$], resulting in a shortened depletion region at the metal-channel interface and thus a higher probability to tunnel through this shorter depletion width as shown in the bottom panel of Fig. S10b. This process would induce a clear bionic current response (such as EPSC, PPF). The strong coupling between the electrical gate and drain terminals will finally result in the superlinear or linear dendritic arithmetics depended on the intensities of driving inputs or modulatory terminal. According to the previous reports, as shown in Fig. S10c below, the superlinear and linear dendritic summation correspond to the biological within-branch and between-branch dendritic summation behavior far away from the soma, respectively.[5, 6]

(ii) Secondly, as a contrast, the Fig. S10d shows a schematic diagram for the two driving inputs based on electrical gate and photonic light. If both the electrical gate and photonic light pulses are applied, the Fermi level will also shift toward the conduction band due to the vertical photo-generated carrier and gating effects, and the source-to-drain energy-band difference will increase to be q[$V_{D(bias)}$], as shown in the Fig. S10e. This synergic effect between the electrical gate and photonic light would finally result in the sigmoidal nonlinear or sublinear dendritic arithmetics depended on the intensities of driving inputs or modulatory terminal. According to the previous reports, as shown in Fig. S10f, the sigmoidal nonlinear and sublinear dendritic summation correspond to the biological within-branch and between-branch dendritic summation behavior near the soma, respectively.[5-7]

(iii) Thirdly, the Fig. S10g shows a schematic diagram for the two driving inputs based on electrical drain and photonic light. If both the electrical drain and photonic light pulses are applied, the Fermi level would shift toward the conduction band due to the lateral photo-generated carrier and bias effects, and the source-to-drain energy-band difference will greatly increase to be q[$V_{D(bias)}$+$V_{D(pulse)}$], as shown in the Fig. S10h. The pitch-off point in the channel will transversely move toward the drain terminal, resulting in a significant EPSC response. This strong synergic effect between the electrical drain and photonic light would finally result in a superlinear dendritic arithmetic regardless of the intensities of driving inputs or modulatory terminal. According to the previous reports, as shown in Fig. S10i below, this superlinear dendritic summation corresponds to the biological within-branch dendritic summation behavior far away from the soma.[5, 6]

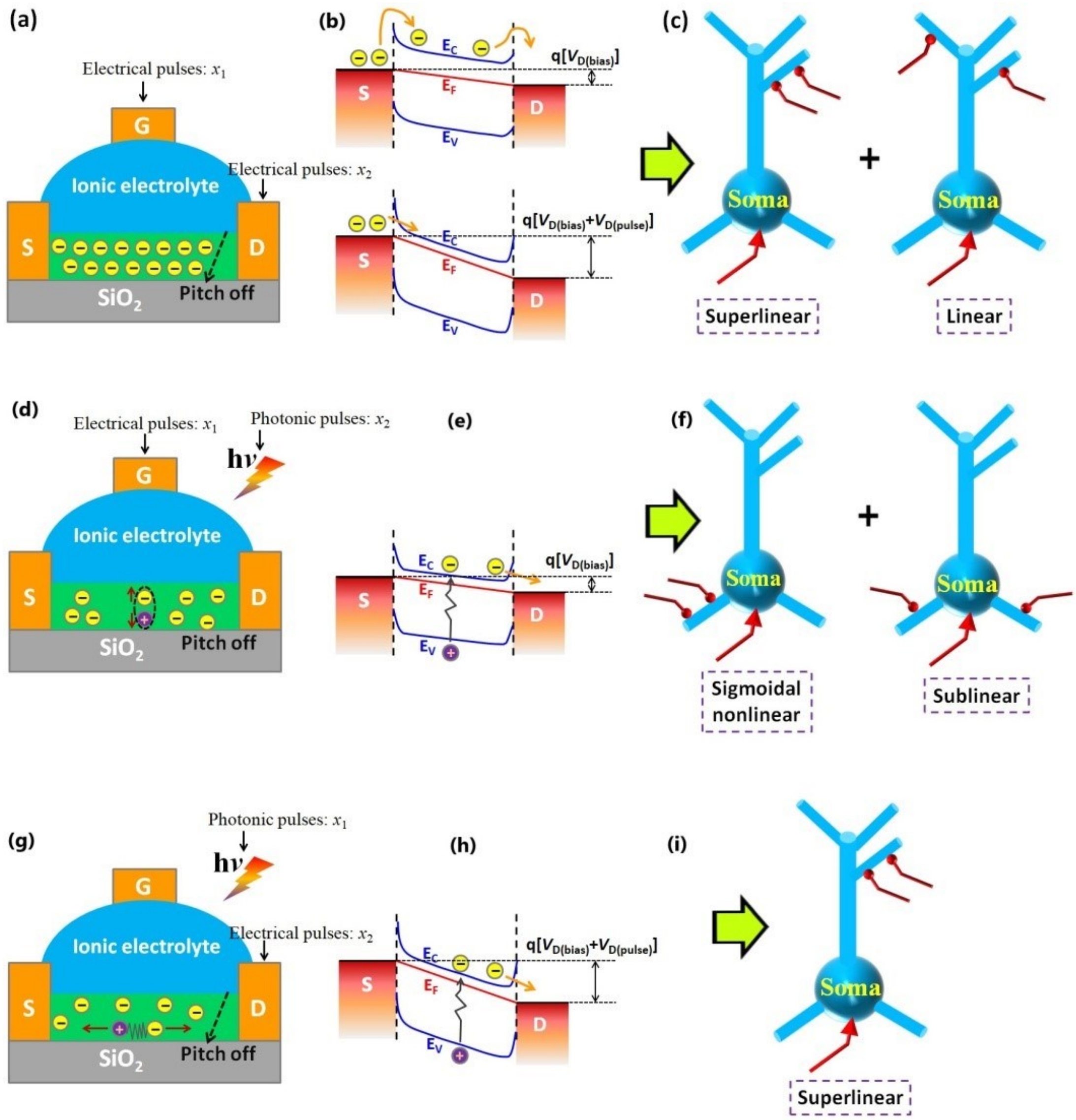

Figure S10: (a~c) For the case of the two driving inputs with electrical gate and drain terminals. (a) A schematic diagram; (b) Top panel: energy diagram for the device without any biases. Bottom panel: energy diagram for the device with two inputs; (c) Corresponding dendritic arithmetics; (d~f) Similar case of the two driving inputs with electrical gate and photonic light terminals; (g~i) Similar case of the two driving inputs with electrical drain and photonic light terminals.

Reference

1. L. Q. Zhu, C. J. Wan, L. Q. Guo, Y. Shi and Q. Wan, *Nat Commun*, 2014, **5**, 3158.
2. O. Larsson, E. Said, M. Berggren and X. Crispin, *Advanced Functional Materials*, 2009, **19**, 3334-3341.
3. S. Das, H. Y. Chen, A. V. Penumatcha and J. Appenzeller, *Nano Lett*, 2013, **13**, 100-105.
4. J. Jiang, A. C. Ahyi and S. Dhar, *IEEE Transactions on Electron Devices*, 2016, **63**, 573-577.
5. P. Poirazi, T. Brannon and B. W. Mel, *Neuron*, 2003, **37**, 977-987.
6. A. Polsky, B. W. Mel and J. Schiller, *Nat Neurosci*, 2004, **7**, 621-627.
7. M. E. Larkum, T. Nevian, M. Sandler, A. Polsky and J. Schiller, *Science*, 2009, **325**, 756-760.